Computers and Concrete, *Vol. 32, No. 5 (2023) 465-474*
https://doi.org/10.12989/cac.2023.32.5.465

A self-confined compression model of point load test and corresponding numerical and experimental validation

Qingwen Shi[1], Zhenhua Ouyang*[1], Brijes Mishra[2] and Yun Zhao[3]

[1]*School of Mine Safety, North China Institute of Science and Technology, Sanhe, Hebei 065201, China*
[2]*Department of Mining Engineering, The University of Utah, Salt Lake City, Utah 84112, USA*
[3]*Department of Mineral Resources, Xingfa Group, Yichang, Hubei 443000, China*

(*Received December 2 2021, Revised December 21, 2021, Accepted June 20, 2023*)

Abstract. The point load test (PLT) is a widely-used alternative method in the field to determine the uniaxial compressive strength due to its simple testing machine and procedure. The point load test index can estimate the uniaxial compressive strength through conversion factors based on the rock types. However, the mechanism correlating these two parameters and the influence of the mechanical properties on PLT results are still not well understood. This study proposed a theoretical model to understand the mechanism of PLT serving as an alternative to the UCS test based on laboratory observation and literature survey. This model found that the point load test is a self-confined compression test. There is a compressive ellipsoid near the loading axis, whose dilation forms a tensile ring that provides confinement on this ellipsoid. The peak load of a point load test is linearly positive correlated to the tensile strength and negatively correlated to the Poisson ratio. The model was then verified using numerical and experimental approaches. In numerical verification, the PLT discs were simulated using flat-joint BPM of PFC3D to model the force distribution, crack propagation and BPM properties' effect with calibrated micro-parameters from laboratory UCS test and point load test of Berea sandstones. It further verified the mechanism experimentally by conducting a uniaxial compressive test, Brazilian test, and point load test on four different rocks. The findings from this study can explain the mechanism and improve the understanding of point load in determining uniaxial compressive strength.

Keywords: laboratory test; numerical simulation; point load test; self-confined compression model

1. Introduction

The uniaxial (unconfined) compressive strength (UCS) test is a widely-used test for rock strength classification (Wang *et al*. 2018). However, it requires well-machined specimens and large testing machines and is, therefore, time-consuming and expensive, essentially confined to the laboratory setting. Researchers have been working on various alternatives to improve the convenience of obtaining UCS (Broch and Franklin 1972). Point load test (PLT), once used as an alternative for direct tensile strength test (Bieniawski 1975, Broch and Franklin 1972), attracts the attention of researchers and engineers due to its high efficiency and simplicity. This test loads the core specimens or irregular rock fragments between the truncated, conical platens (ASTM standard D5731-16 2016) at failure. Then the peak load, specimen size, specimen shape, and loading mode become variables to calculate the point load strength index ($I_{s(50)}$). Previous studies validated that the UCS σ_c can be derived through the equation $\sigma_c = CI_{s(50)}$, where C is a constant depending on rock type, after observing large amount of tests results with various rock type (ASTM standard D5731-16 2016, Broch and Franklin 1972, Franklin 1985, Wen *et al*. 2019).

There has been significant research on the procedures for this test and proper value for the constant C for different types of rock (Kaya and Karaman 2016, Sarici and Ozdemir 2018, Wong *et al*. 2017, Yin *et al*. 2017). Since the specimens in PLT can be both irregular and cylinder-shaped, researchers have also studied the size and shape effects in PLT extensively (Kabilan *et al.* 2017, Şahin *et al.* 2020, Wei *et al.* 2019, Xue *et al.* 2018). Some researchers began to pay attention to the failure mode of point load test with different rock types (Basu *et al.* 2013, Everall and Sanislav 2018). The difference between the isotropic and schist rocks were mainly discussed. Zhang (2016) adopted PLT to analyze the strength anisotropy of DanBa quartz mica schist. Two types of failure modes have been observed by Zhang according to the fracture orientation to bedding layers.

However, despite the numerous efforts that were made to apply this method as an alternative to the UCS test, only a few attempted to understand the mechanism behind these applications. Serati (2018) used the point load index to measure the tensile strength of rock, concluding that the induced tensile stress at the center of a diametral point load specimen as well as the point load strength index is a function of both Poisson's ratio and sample length. Hoek (1977) indicated that the mechanics of the PLT cause the rock to fail in tension. He provided the stress-induced at the center of a disc of diameter D and thickness t as a result of the application of a diametrically opposed point load P. Hoek claimed that the ratio between the tensile strength and

*Corresponding author, Professor
E-mail: oyzhua@163.com

Copyright © 2023 Techno-Press, Ltd.

ISSN: 1598-8198 (Print), 1598-818X (Online)

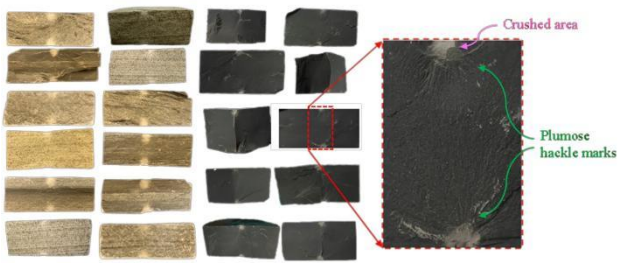

Fig. 1 Fracture surface morphology variation along the loading axis

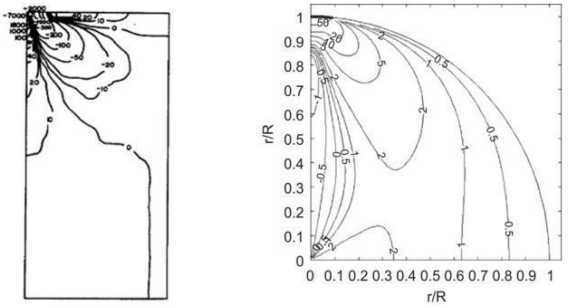

(a) Cylindrical specimen (Peng 1976) (b) Spherical specimen (Russell and Muir Wood 2009)

Fig. 2 2D stress field

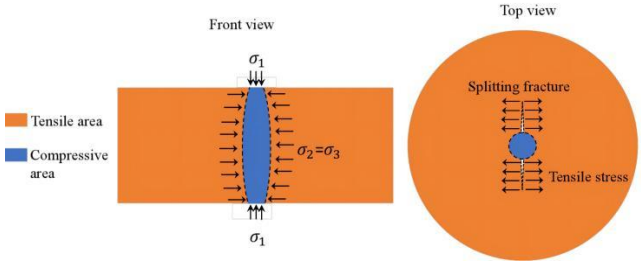

Fig. 3 Front and top view of the cross-section of the distribution of the sample

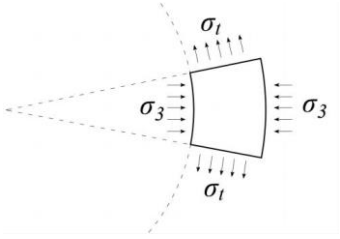

Fig. 4 Stress state of the unit on the inner edge of the tensile ring

compressive strength stays stable for a particular brittle rock, and thus one can obtain the compressive strength by this ratio. Hoek's work sheds light on the mechanisms of the PLT to reveal the compressive strength, leading researchers to realize the significance of the stress field in the PLT disc when evaluating the strength of the rocks. However, many researchers have recognized that the contact area between the truncated conical loading machine and the disc is a circle area instead of a perfect point. The area also varies with different types of rocks. The loading area can make a big difference in theoretical derivation, which was not considered in Hoek's hypothesis.

It is noted that previous studies are mainly concerned with the practical application of this PLT. Few investigations paid attention to the intrinsic mechanism of the point load test's capacity to reveal the UCS strength. The present study attempts to fill the gap by proposing a theoretical model of the PLT mechanism based on a large number of laboratory observations and existing research as well. The model was systematically verified with numerical and experimental methods. This study will further enhance the understanding of the mechanism of using PLT as an alternative to the uniaxial compressive test.

2. Self-confined compression model of PLT

For understanding the intrinsic mechanism of a PLT disc failure, surface analysis was conducted on a large number of failed specimens. A typical obvious plumose arrangement (Xie *et al.* 1999) of hackle marks was observed at the contact points of the platen with the specimen, as shown in Fig. 1. The white semicircular area in Fig. 1 is the crushed area by the point load around which the hackle marks are radially distributed. These hackle marks are indicative of tensile failure according to fracture surface analysis theory (Lutton 1970, Lutton 2006, Xie *et al.* 1999). The tensile failure near the contacting point was more clearly illustrated using photoelasticity conducted by Frocht (1974). However, Fig. 1 shows that the plumose arrangement disappears in the area far from the loading axis of the specimen, indicating a different failure mechanism in this area.

Literature survey implies that the different failure mechanisms that occurred in the area far from the loading axis could be a tensile stress-induced failure. For example, Peng (1976) pointed out the majority of the specimen is in a compressive state as shown in Fig. 2(a). This was further verified by a reported observation of the stress field in a PLT specimen (Russell and Muir Wood 2009). Russel and Wood (2009) exhibited an ellipsoid-shaped compressive zone along the loading axis in an elastic sphere, as shown in Fig. 2(b). Both investigations showed that the maximum tensile stress occurs around the loading point. This tensile stress decreases rapidly and becomes compressive stress in the central portion of the specimen but exists in the area far from the axis. The findings can perfectly explain the disappearance of the plumose arrangement observed in Fig. 1.

Based on the laboratory observation and existing research above, it is found that the rock around the loading axis (named the near-axis rock here) is actually in a compressive state (see Fig. 3); According to the shape of hackle marks in Fig. 1 and stress distribution in Fig. 2, the compressive zone is assumed as an ellipsoid in the present study. Due to the Poisson effect, the rock mass composing the ellipsoid dilates under the compressive stress, which introduces tensile strain and stress in the rock slightly further from the loading axis. The tensile zone forms a ring as shown in Fig. 3. Meanwhile, the far-axis rock provides confining stress to the ellipsoid as reaction stress and formed a self-confined compression model depicted in Fig.

3. Based on this model, the correlation between the point load test result and the rock mass's mechanical properties are analyzed.

Taking the unit located at the inner edge of the tensile ring out for stress analysis (see Fig. 4), one can see the stress state of a rock unit where tensile failure happens.

According to the elastic-plastic mechanism,

$$\sigma_t = -\sigma_3 \cdot N_\varphi + 2c \cdot N_\varphi \tag{1}$$

$$N_\varphi = \frac{1+\sin\phi}{1-\sin\phi} \tag{2}$$

Where c is cohesion of the rock and φ denotes friction angle of the rock.

At the point of failure, the tensile stress will reach the tensile strength

$$\sigma_t = [\sigma_t] \tag{3}$$

Thus,

$$\sigma_3 = 2c - \frac{1}{N_\varphi} \cdot [\sigma_t] \tag{4}$$

Assuming the axial strain is ε_1, the lateral strain will be $\varepsilon_2 = \mu\varepsilon_1$, and the strain of the tensile ring (occurring in the edge of the ring) will be $\varepsilon_r = \varepsilon_2$. So the maximum tensile stress can be deduced as

$$[\sigma_t] = E \cdot \varepsilon_r = E \cdot \varepsilon_2 = \mu E \cdot \varepsilon_1 \tag{5}$$

The axial strain of compressive ellipsoid will be

$$\varepsilon_1 = \frac{1}{E}[\sigma_1 - \mu(\sigma_2 + \sigma_3)] = \frac{1}{E}[\sigma_1 - 2\mu \cdot \sigma_3] \tag{6}$$

With Eqs. (5) and (6), the relationship between $[\sigma_t]$ and σ_1 can be demonstrated as

$$\sigma_1 = \frac{1}{\mu} \cdot [\sigma_t] + 2\mu \cdot \sigma_3 \tag{7}$$

So the relationship with a loading stress σ_1 and tensile strength of the rock disc can be derived as

$$\sigma_1 = \left(\frac{1}{\mu} - \frac{2\mu}{N_\varphi}\right) \cdot [\sigma_t] + 4\mu \cdot c \tag{8}$$

Assuming the contact area with the loading machine and disc as A, the peak load can be expressed as

$$P_{max} = A \cdot \sigma_1 = \left(\frac{A}{\mu} - \frac{2A\mu}{N_\varphi}\right) \cdot [\sigma_t] + 4A\mu \cdot c \tag{9}$$

According to this discussion, the ellipsoid is experiencing a confined compressive test; the confinement is actually caused by itself, referred to as a self-confined compression test. The peak load of a point load test is linearly positive correlated to the tensile strength of the sample. Based on this, the point load test can reveal the confined compressive strength of the rock mass under confining stress determined by its tensile strength. In order to verify the Eq. (9) deduced from the proposed self-confined compression model, numerical modeling and laboratory test are conducted in the following sections.

3. Validation of self-confined compression model with bonded particle material

To check the self-confined compression model, a series of numerical modeling was conducted using Particle Flow Code 3D (PFC3D) (Itasca Consulting Group 2019). In the modeling, bonded particle material (BPM) capable of replicating Berea sandstone behavior was firstly generated. The radii increase technique was used for creating the BPM. Specifically, we first created a material vessel consisting of six walls. The particles were then created with diameters satisfying a uniform particle-size between minimum radius and maximum radius. Then the particle radii were increased to their final values with no overlap. Secondly, using the generated BPM, the force distribution and crack propagation during the point load test were probed and discussed in comparison with the self-confined compression model. Then the material properties' effect on the PLT results are verified against Eq. (9) deduced from the self-confined compression model above.

3.1 Generation of the PLT disc with BPM

PFC3D, a discrete-element method (DEM), was adopted due to its advantage over continuum modeling in modeling fracture damage (Shi and Mishra 2020, Shi *et al.* 2022). The BPM in PFC models the intact rock and introduces the mechanical behavior of the fractures by modifying the contact models at contacts intercepting fractures (Koyama and Jing 2007).

To generate the PLT disc with the capacity to replicate the behavior of actual rock mass, the BPM was calibrated upon laboratory tests with Berea sandstone. The procedure and results of the calibration and the PLT disc are illustrated in this section.

3.1.1 Laboratory tests on Berea sandstones

The point load test is known as not applicable for soft rocks. The ASTM standard (ASTM standard D5731-16 2016) indicates that this method should be applied only to medium-strength rock whose compressive strength is greater than 15MPa. Therefore, this research performed tests on Berea sandstone specimens, quarried from the Northern Ohio deposits of Cleveland Quarries. Made up of well-sorted and well-rounded predominately quartz grains (Churcher *et al*. 1991), the Berea sandstone is well known as highly homogenous, well-characterized, and readily available. Because of all the above features, Berea sandstone has been widely used in geological research for years as a standard material in core analysis research.

With the selected Berea sandstone, the lab ran three groups of UCS tests (see Table 1) and four groups of point load tests (see Table 2) according to the ASTM standard (ASTM standard D5731-16 2016). When using point load test as an alternative of UCS test, there exists a large variability of point load test results due to defects in the specimen and size effect as well. Therefore, different sizes of point load test specimens are usually used to eliminate influence of these external factors. Considering replicating actual scenarios of performing point load test, point load test was conducted on discs with different thicknesses for following calibration. Besides, the more models calibrated, the more accurate the micro-parameters can reproduce the real rock. The MTS servo-controlled compression testing

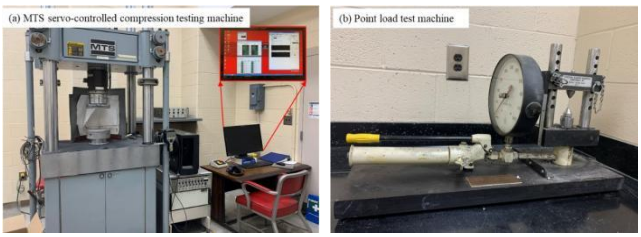

(a) MTS servo-controlled compression testing machine (b) Point load test machine

Fig. 5 Test machines for UCS test and point load test

Table 1 UCS test results

Specimen #	Uniaxial compressive strength (MPa)	Young's Modulus (GPa)
1	63.7	11.3
2	65.7	10.0
3	58.1	10.2
Avg.	62.5	10.5

Table 2 Point load test results

Thickness (mm)	Specimen #	Peak load (N)
19	A-1	2872.5
	A-2	1888.4
	A-3	4174.5
21	B-1	4621.8
	B-2	4124.8
	B-3	4671.5
27	C-1	4671.5
	C-2	4025.4
	C-3	5466.7
34	D-1	6013.3
	D-2	5665.4
	D-3	-

machine and point load test machine, as shown in Fig. 5, conducted these tests for calibration. The displacement of the loading platen of MTS servo-controlled compression testing machine was monitored to obtain the axial strain of the samples.

Table 1 and Table 2 showed the test results and Fig. 6 shows the failed specimens in laboratory tests.

3.1.2 Calibration of the BPM

The 3D BPM micro-parameters were determined by demonstrating that the material matches much of the response obtained during the UCS tests and PLT of a typical compact rock-in this case, Berea sandstone. Flat-jointed constitutive model was used to generate the BPM. The BPM UCS test and PLT with various disc thicknesses were all used for calibration.

The dimension of the UCS test model was consistent with the specimens used in the lab, with a diameter of 54.1 mm and a length of 116.1mm. Additionally, the thickness of the point load test models was set to be the same as

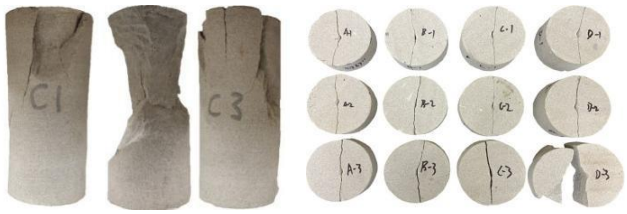

(a) Uniaxial compressive test (b) Point load test

Fig. 6 Berea sandstone failure

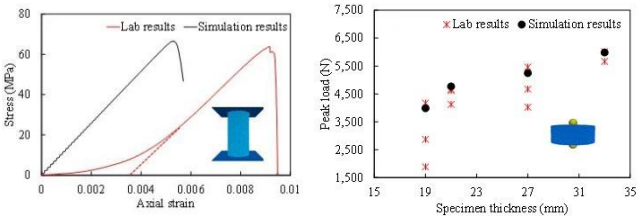

(a) Uniaxial compressive test (b) Point load test

Fig. 7 Calibration results

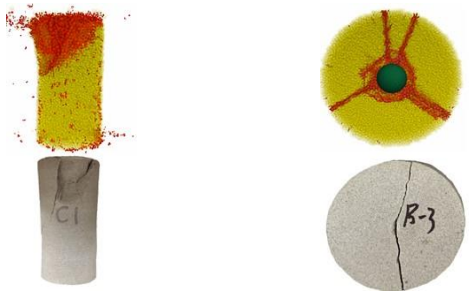

(a) Uniaxial compressive test (b) Point load test

Fig. 8 Comparison between numerical and laboratory failure mode

laboratory specimens, which is 19 mm, 21 mm, 27 mm, and 33 mm, respectively. The diameter was set at 54.1 mm. Porosity ratio in PFC3D, defined as the ratio of the volume of pores to the volume of bulk BPM, not only presents the geometric distribution of the particles but also pose significant impact on the mechanical behavior of the BPM. In the present numerical study, the porosity ratio of 0.2 recommended by Potyondy (2018) for sedimentary rock was used. The minimum radius of the particle assembly was 0.5 mm, and the particle size ratio was 1.5. The stiffness ratio was 1.0. The particle radii were set to have a uniform distribution in these samples. The wall, which is a rigid element in PFC, simulated the platen in the UCS test and the loading indenters in PLT. In this research, a 5-mm radius spherical indenter was used to simulate the indenters (ASTM standard D5731-16 2016).

Through multiple cycles of trial and error, the determined parameters were obtained. Fig. 7(a) shows the calibrated and laboratory strain-stress curve for the UCS test. The predicted Young's modulus and UCS are 12.9 GPa and 66.5 MPa, which are in good agreement with the laboratory results. The difference in the behavior of the model and laboratory test is the absence of nonlinear behavior at the beginning of the test. Heterogeneity and pores present in the actual rock cause some initial

Table 3 Parameters used to calibrate the model

Parameter	Physical meaning	Value
porosity	Porosity ratio	0.2
fj_radius	Minimum radius of the particle (mm)	0.5
	Maximum radius of the particle (mm)	0.75
fj_kratio	Normal-to-shear stiffness ratio	1.0
fj_fric	Friction coefficient	0.577
fj_emod	Effective modulus (GPa)	7.0
fj_ten	Tensile strength (MPa)	1.837
fj_fa	Friction angle (degrees)	25
fj_coh	Cohesion (MPa)	17.11

compaction resulting in the nonlinear behavior in a laboratory specimen (Jaeger *et al.* 2009). Fig. 7(b) shows the comparison between numerical results and laboratory results of PLT for specimens with varied thicknesses. It is observed that the macro properties from the numerical tests matched the laboratory tests.

The comparison between the numerical and laboratory failure patterns is shown in Fig. 8. The yellow particles, set as translucent, represent the assembly of the sample while the red disks represent the cracks caused by the loading process. The green sphere in Fig. 8(b) represents the indenter. The failure modes in the numerical model matched well with experimental observations. The laboratory PLT specimen failed along a single plane while the numerical model followed a multi-plane mode. Both failure modes are accepted as per ASTM standard (ASTM standard D5731-16 2016) and various published literature (Basu *et al.* 2013, Everall and Sanislav 2018). In general, the failure mode further validated the reliability of the numerical models in this study. The BPM models in PFC3D can capture the fracturing behavior of the Berea sandstone. The parameters adopted in the BPM are listed in Table 3.

3.2 Force distribution and crack propagation during a PLT

Observing the stress/force distribution and crack propagation process plays a key role in unstanding the mechanism of PLT. In this section, the calibrated micro-parameters derived above were used for these investigations.

3.2.1 Force distribution

Fig. 9 presents the force distribution in the point load test disc before failure. The compressive and tensile forces are generated in different colors—red and green, respectively. The boldness of the force chain represents the magnitude of the force. This figure illustrates that the distribution feature of the force is distinctive. The compressive force is mainly distributed around the loading axis in an ellipsoid shape with relatively high magnitude, referred to as a compressive ellipsoid. The highest compressive force occurs at the elements immediately next to the loading point, decreasing rapidly as it moves toward the interior of the specimen. Meanwhile, outside of the

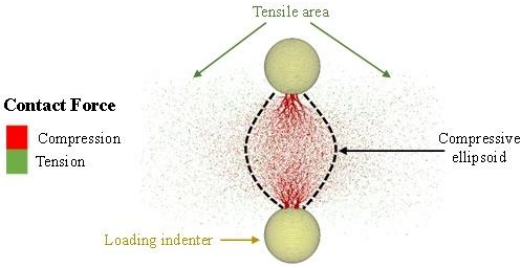

Fig. 9 The force chain in the point load test sample (the black dashed line illustrates the approximate location and shape of the compressive ellipsoid)

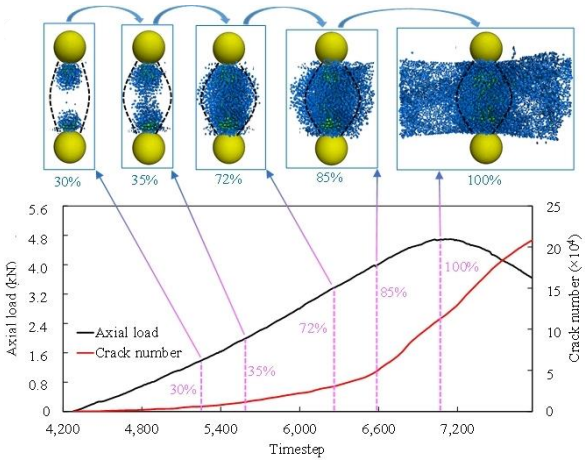

Fig. 10 The load and crack number variation and corresponding crack propagation during a point load test (the pink dashed lines represent the load level (in percentage of peak load) at which the crack propagation is extracted; the blue flakes represent the tensile cracks while the green ones represent shear cracks; the black dashed lines represent the shape and location of the compressive ellipsoid; the yellow spheres are the loading indenters)

ellipsoid, tensile areas are present around with a lower magnitude than the compressive force. This scenario agrees well with the self-confined model proposed in Section 2.

3.2.2 Crack propagation

BPM discs of 21mm-thickness were used for crack propagation observation. Fig. 10(a) shows the axial load-timestep curve and crack number-timestep curve throughout the point load test. As seen in this cumulative crack plot, most fracturing surges around 85% of the peak load. Typical crack propagation scenario during the test were extracted at 30%, 35%, 72%, 85% and 100% of the peak load respectively as shown in Fig. 10(b). This figures depict the crack distributions as bi-colored flakes in which green represents shear-induced failure and blue represents tension-induced failure. The loading indenters are depicted as a pair of yellow spheres. The black dashed lines in Fig. 10(b) depicts the shape and location of the compressive ellipsoid at various load levels.

Fig. 10(b) shows that the cracks initiate at the loading points at 30% of the peak load, with few cracks. During this stage some shear cracks develop around the loading points. With the increase in the load, the cracks extend along the

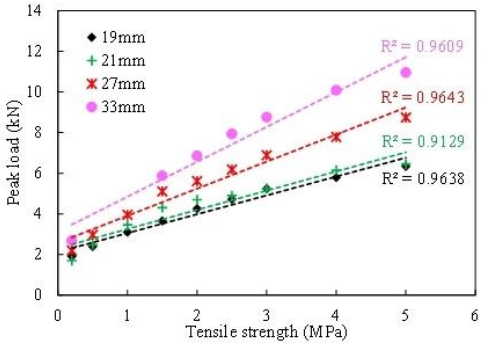

Fig. 11 Fitting results for peak load versus tensile strength for discs with various thickness

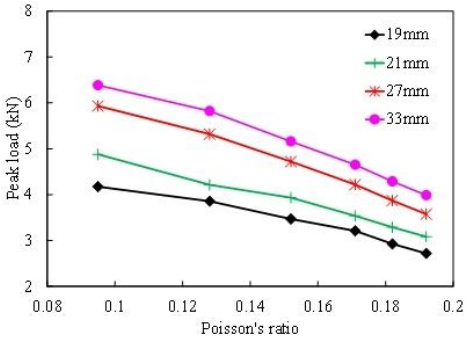

Fig. 12 Relationship between PLT peak load and Poisson's ratio of the BPM

loading axis, as shown at 35% and 72% of the peak load. And only tensile cracks propagate through the specimen. Upon the 72% of the peak load, the cracks are evenly distributed along the loading axis, and the upper and lower cracks connect to each other. The trend that cracks starts from loading ends and develop toward the central portion agrees well with the typical numerical results of the compressive test (Yoon 2007, Zhang *et al*. 2019). At the same time, it is observed the cracks are distributed within the range of the compressive ellipsoid which is shown by the black dashed lines when the load is less than 72% of the peak load. This stage corresponds to the rock dilation under the compressive stress as described in the self-confined compression model in Section 2.

When the test reached 85% of the peak load at which the crack number surges, the splitting cracks develop in the specimen. With the increase in the load, the splitting cracks continue to extend forward to the edge of the disc. When the load increases to 100% of peak load, all the splitting cracks reach the edge and the disc is thoroughly penetrated. At this point, the compressive ellipsoid zone loses its confinement applied by the tensile area and the disc was fully split into fragments. The cracking propagation with the load development is observed to agree with the self-confined compression model.

3.3 BPM properties' effect on PLT results

Based on the self-confined compression model, the PLT peak load is linearly positive to the tensile strength of the rock mass. And the tensile failure in the PLT disc is actually induced by the dilation of the near-axis rock. Poisson's ratio is known to affect the degree of dilation. To verify the self-confined compression model put forward above, the generated BPM was used to model the mechanical relation between peak load with Poisson's ratio and the tensile strength.

3.3.1 PLT peak load and the tensile strength

The tensile strength can be changed directly using the program's internal language (FISH) in the PFC model. The thickness of the specimen was maintained to be the same with laboratory specimens, which are 19 mm, 21 mm, 27 mm, and 34 mm, respectively. For each thickness, BPM with tensile strength of 0.2 MPa, 0.5 MPa, 1.0 MPa, 1.5 MPa, 2.0 MPa, 2.5 MPa, 3.0 MPa, 4.0 MPa and 5.0 MPa were generated and compressed to failure with point load test in sequence.

Fig. 11 shows the curve fitting result for the relation between peak load and tensile strength for specimens with different thicknesses. The R2 represents the coefficient of determination of the fitting trendlines. This figure clearly shows that for each thickness, when other properties remain unchanged, the peak load of the point load tests are linearly positive correlated to the tensile strength of the disc. The linear lines perfectly fit the scatter points, indicating that the mathematical relation of numerical simulations agrees well with the Eq. (9) attained from self-confined compression model.

3.3.2 PLT peak load and the tensile strength

Poisson's ratio determines the extent of the dilation. This section investigates the impact of Poisson's ratio on the peak load of the point load using a BPM disc with the thickness of 19 mm, 21 mm, 27 mm, and 34 mm, respectively.

In PFC, the Poisson's ratio (v) can be defined directly by the normal-to-shear stiffness ratio (fj_kratio in Table 3). v is related to stiffness ratio fj-kratio with v increasing as fj-kratio increases (Itasca Consulting Group 2019, Potyondy 2017). The fj_kratio was varied from 1.5 to 4.0 with an interval of 0.5 because the fj_kratio is normally set no larger than 4.0 in BPM models. Accordingly, BPM with different Poisson's ratios, whose calculation was coded into the PFC3D model, was obtained and then used to conduct PLT. Fig. 12 shows the relationship between peak load and Poisson's ratio of discs with different thicknesses.

It is observed the peak load decreases monotonically with the Poisson's ratio of the models for a specific thickness. This verifies the PLT self-confined compression model wherein the dilation of compressive ellipsoid causes tensile stress and finally leads to failure. The larger the Poisson's ratio, the more the compressive ellipsoid will dilate under a specific load and the larger tensile stress will be induced. The PLT peak load will be reached once the tensile strength is exceeded by this induced tensile stress as depicted in the self-confined compression model.

4. Experimental validation of self-confined

compression model

To experimentally verify the self-confined compression model, the effect of rock's properties, i.e., tensile strength and Poisson's ratio, on the PLT results was evaluated by testing specimens of different rock types. These tests included four different types of rocks: Marcellus shale, gray sandstone, white sandstone, and Berea sandstone. Marcellus shale is a part of the sedimentary system known as the Appalachian Basin. The gray and white sandstone used in the research was cored from different locations of an underground coal mine in Pennsylvania, US. All the specimens used in this research were fine-grained without inclusions.

4.1 Experiment setup

Three types of tests, i.e., UCS test, Brazilian test, and PLT, were performed on each rock type to determine the material's Poisson ratio, tensile strength, and corresponding PLT peak load. The UCS test specimens were standard UCS cylinders with a diameter of 54 mm and a height of greater than 108mm (a height to diameter ratio of larger than 2.0). The circumferential extensometer was used for measuring the lateral strain in the cylindrical specimen. The prepared Brazilian test specimens were standard discs with a diameter of 54 mm and a thickness of 27 mm (diameter to thickness ratio of 0.5). All the PLT specimens were set at a diameter of 54 mm and a thickness of 25 mm. MTS planar platens, standard Brazilian jaws, and truncated conical indenters applied the load, respectively, as per the ASTM standards (ASTM Standard D3148-02 2002, ASTM Standard D3967-16 2016, ASTM standard D5731-16 2016), as shown in Fig. 13. For each rock type, we conducted two groups of UCS tests, five groups of Brazilian tests, and three groups of PLT. The displacement control mode was utilized in both UCS tests and Brazilian tests. Specificly, an axial displacement rate of 0.2 mm/min was used in the UCS tests and an axial displacement rate of 0.1 mm/min was used in the Brazilian tests. These loading rates guaranteed that the failure occurs within required test time, which is 2 to 15 min for UCS test and 1 to 10 min for Brazilian test. In the Brazilian test, the displacement control mode was realized by controlling the plate displacement rate.

4.2 Laboratory results and discussion

The Poisson's ratio and tensile strength of each rock type were calculated using the formula given by ASTM standards (ASTM Standard D3148-02 2002, ASTM Standard D3967-16 2016, ASTM standard D5731-16 2016). When calculating the Poisson's ratio, the lateral strain which was obtained by the circumferential extensometer has to be used. However, it has been identified that the circumferential extensometer causes an error varying from 5% to 9% because it does not include the complete perimeter of the test cylinder (Masoumi *et al.* 2015), as shown by the gap formed by both ends of the chain in Fig. 14. For accuracy of verifying the relationship between PLT results and Poisson' ratio, the calculation of the lateral strain

Fig. 13 Loading conditions of UCS test, Brazilian test, and PLT

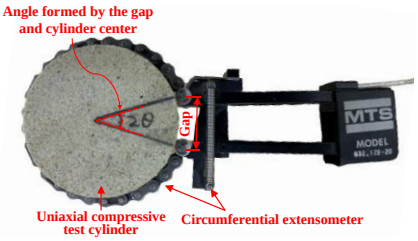

Fig. 14 Attachment between the extensometer and the 54-mm-diameter specimen

Table 4 Test results of selected rocks

	Poisson's ratio	Tensile strength (MPa)	PLT peak load* (kN)
Marcellus shale	0.22	7.54	14.67
	0.24	5.52	13.10
		6.70	12.58
		8.23	
		7.49	
	Avg.=0.23	Avg.=7.10	Avg.=13.45
Gray sandstone	0.12	14.59	28.12
	0.12	13.78	18.86
		12.55	17.82
		11.54	
		14.13	
	Avg.=0.12	Avg.=13.32	Avg.=21.60
White sandstone	0.06	13.22	26.90
	0.08	13.95	26.03
		16.37	25.33
		14.48	
		14.72	
	Avg.=0.07	Avg.=14.55	Avg.=26.08
Berea sandstone	0.28	4.22	10.48
	0.27	4.16	9.61
		4.57	8.73
		3.95	
		-	
	Avg.=0.275	Avg.=4.23	Avg.=9.61

*All the PLT results were obtained from discs with an identical thickness of 21 mm.

was modified with a modification factor of c=0.957 obtained from the formula given below (Masoumi *et al.* 2015)

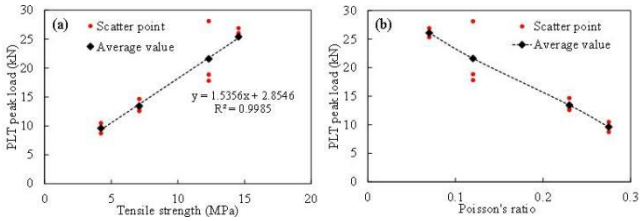

(a) Tensile strength (b) Poisson's ratio

Fig. 15 The variations of PLT peak load versus

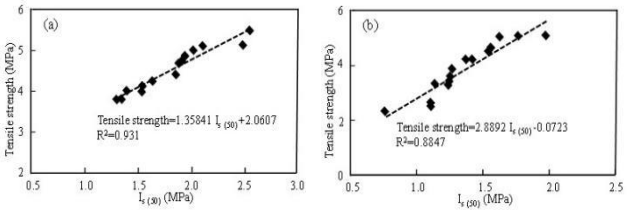

(a) Air-dried gypsum rock (b) Saturated gypsum rock

Fig. 16 Tensile strength versus $I_{s(50)}$

$$c = \frac{2\sin\theta + 2\cos\theta(\pi - \theta)}{2\pi} \quad (10)$$

Where θ denotes half the angle formed by the gap the center of the cylinder as shown in Fig. 14. It was measured as 17.5˚ in our laboratory tests here.

Table 4 gives the details of the test results of the Poisson's ratio, Brazilian tensile strength and corresponding PLT results of each rock type.

The PLT test results were plotted against the rock's tensile strength and Poisson's ratio, respectively, as shown in Fig. 15. The black dashed lines in Fig. 15 presents the linear trendline of the average PLT peak load against the tensile strength (Fig. 15(a)) and the Poisson's ratio (Fig. 15(b)). Excluding the impacts of other mechanical parameters, the PLT peak load is linearly positive correlated to the tensile strength, verifying the Eq. (9) deduced from self-confined compression model in Section 2 and the numerical results. Similarly, Fig. 15(b) shows that the PLT peak load is negatively related to the Poisson's ratio, which is also in agreement with Eq. (9) and the numerical results.

Generally, results from the experimental and numerical analysis both verified the self-confined compression model proposed in the present research. In fact, the linear relation between PLT peak load and the rock's tensile strength can also be validated from the published literature. In an expression $T=KP/h^2$ proposed by Timoshenko and Goodier (1951), where T is tensile strength, K is constant, P is PLT peak load and h is the height of the PLT disc, the tensile strength is linearly positive correlated to the PLT peak load. This expression was substantiated by the work of Sternberg and Rosenthal (1952). Besides, Heidari *et al*. (2012) experimentally proved that the PLT strength index $I_{s(50)}$ is linearly correlated to the Brazilian tensile strength of gypsum rocks with different moisture conditions, as shown in Fig. 16. $I_{s(50)}$ is proportional to the PLT peak load for a specific dimension, indicating that the gypsum rocks' PLT peak load is linearly correlated to its tensile strength.

5. Conclusions

This study proposed a theoretical model to understand the mechanism of PLT serving as an alternative to the UCS test based on laboratory observation and literature survey. The model was then verified using numerical and experimental approaches.

The fracture surface morphology on a large number of PLT indicates that there is a compressive area along the loading axis but turned into tensile stress in the area far from the loading axis. Combined with existing research, a self-confined compression model of PLT was proposed. According to the proposed model, the compressive stress is distributed around the loading axis in an ellipsoid shape. Outside of the ellipsoid, there is a ring-shaped area present around. The ring-shaped area is in a tensile state due to the dilation of the ellipsoid and it applies the confined stress to the ellipsoid. Based on this interaction between the compressive ellipsoid and tensile ring, the model demonstrates that the peak load of a point load test correlates positively with the tensile strength of the rock.

Using the BPM of PFC3D which was calibrated based on laboratory tests upon Berea sandstone, the self-confined compression model was verified. Numerical results showed that the compressive force is distributed around the loading axis. The circular tensile zone surrounds the compressive zone. In addition, the propagation of the cracks in the PLT disc to the load variation was numerically compared. The process from initiation of splitting fractures to fully failure of the disc agrees well with the self-confined compression model. The effect of tensile strength and Poisson's ratio on the PLT results were also found to be in good consistency with the self-confined compression model. The Poisson's ratio, Brazilian tensile strength and PLT peak load of four rock types were measured to verify the self-confined compression model experimentally. Results showed that among those four rock types, the PLT peak loads increased linearly with their tensile strength while decreased with their Poisson ratio, validating the proposed model. The relation between PLT peak load and tensile strength was also validated by results from published literature. These results are in good agreement with numerical results and they both validated the self-confined compression model. This study provides a reasonable explanation for the mechanism of deducing UCS with PLT, and others can further study the application based on this mechanism.

Acknowledgments

The research described in this paper was financially supported by the National Nature Science Foundation of China [Grant No.52274120].

References

ASTM Standard D3148-02 (2002), Standard Test Method for

Elastic Moduli of Intact Rock Core Specimens in Uniaxial Compression, American Society for Testing and Materials,West Conshohocken, PA, USA.

ASTM Standard D3967-16 (2016), Standard Test Method for Splitting Tensile Strength of Intact Rock Core Specimens, American Society for Testing and Materials, West Conshohocken, PA, USA.

ASTM standard D5731-16 (2016), Standard Test Method for Determination of the Point Load Strength Index of Rock and Application to Rock Strength Classifications, American Society for Testing and Materials, West Conshohocken, PA, USA.

Basu, A., Mishra, D.A. and Roychowdhury, K. (2013), "Rock failure modes under uniaxial compression, Brazilian, and point load tests", *Bull. Eng. Geol. Environ.*, **72**, 457-475. https://doi.org/10.1007/s10064-013-0505-4.

Bieniawski, Z.T. (1975), "The point-load test in geotechnical practice", *Eng. Geol.*, **9**(1), 1-11. https://doi.org/10.1016/0013-7952(75)90024-1.

Broch, E. and Franklin, J.A. (1972), "The point-load strength test", *Int. J. Rock Mech. Min. Sci. Geomech. Abstr.*, **9**(6), 669-676. https://doi.org/10.1016/0148-9062(72)90030-7.

Churcher, P.L., French, P.R., Shaw, J.C. and Schramm, L.L. (1991), "Rock properties of Berea sandstone, Baker dolomite, and Indiana limestone", *The SPE International Conference on Oilfield Chemistry,* Anaheim, CA, USA, February.

Everall, T.J. and Sanislav, I.V. (2018), "The influence of pre-existing deformation and alteration textures on rock strength, failure modes and shear strength parameters", *Geosci.*, **8**(4), 124. https://doi.org/10.3390/geosciences8040124.

Franklin, J.A. (1985), "Suggested method for determining point load strength", *Int. J. Rock Mech. Min. Sci. Geomech. Abstr.*, **22**(2), 51-60. https://doi.org/10.1016/0148-9062(85)92327-7.

Frocht, M.M. (1974), *Photoelasticity*, Wiley, Hoboken, NJ, USA.

Heidari, M., Khanlari, G.R., Torabi Kaveh, M. and Kargarian, S. (2012), "Predicting the uniaxial compressive and tensile strengths of gypsum rock by point load testing", *Rock Mech. Rock Eng.*, **45**, 265-273. https://doi.org/10.1007/s00603-011-0196-8.

Hoek, E. (1977), "Rock mechanics laboratory testing in the context of a consulting engineering organization", *Int. J. Rock Mech. Min. Sci. Geomech. Abstr.*, **14**(2), 93-101. https://doi.org/10.1016/0148-9062(77)90201-7.

Itasca Consulting Group, Inc. (2019), PFC|US Minneapolis - Itasca Consulting Group, Inc, Itasca Consulting Group, Inc., Minneapolis, MN, USA. https://www.itascacg.com/software/PFC

Jaeger, J.C., Cook, N.G. and Zimmerman, R. (2009), *Fundamentals of Rock Mechanics*, Wiley, Hoboken, NJ, USA.

Kabilan, N., Muttharam, M. and Elamathi, V. (2017), "Prediction of unconfined compressive strength for jointed rocks using point load index based on joint asperity angle", *Geotech. Geol. Eng.*, **35**, 2625-2636. https://doi.org/10.1007/s10706-017-0266-0.

Kaya, A. and Karaman, K. (2016), "Utilizing the strength conversion factor in the estimation of uniaxial compressive strength from the point load index", *Bull. Eng. Geol. Environ.*, **75**, 341-357. https://doi.org/10.1007/s10064-015-0721-1.

Koyama, T. and Jing, L. (2007), "Effects of model scale and particle size on micro-mechanical properties and failure processes of rocks—a particle mechanics approach", *Eng. Anal. Bound. Elem.*, **31**(5), 458-472. https://doi.org/10.1016/j.enganabound.2006.11.009.

Lutton, RJ. (1970), "Tensile fracture mechanics from fracture surface morphology", *The 12th U.S. Symposium on Rock Mechanics*, Rolla, MO, USA, November.

Lutton, R.J. (2006), "Fracture surface morphology", *Structural Geology and Tectonics*, Encyclopedia of Earth Science Springer, Berlin, Heidelberg.

Hossein, M., Paul, C.H. and Serkan, S. (2015), "A modification to radial strain calculation in rock testing", *Geotech. Test. J.*, **38**(6), 813-822. https://doi.org/10.1520/GTJ20140238.

Peng, S.S. (1976), "Stress analysis of cylindrical rock discs subjected to axial double point load", *Int. J. Rock Mech. Min. Sci. Geomech. Abstr.*, **13**(3), 97-101. https://doi.org/10.1016/0148-9062(76)90426-5.

Potyondy, D.O. (2017), "Simulating perforation damage with a flat-jointed bonded-particle material", *The 51st U.S. Rock Mechanics/Geomechanics Symposium*, San Francisco, CA, USA, June.

Potyondy, D.O. (2018), "A flat-jointed bonded-particle model for rock", *The 52nd U.S. Rock Mechanics/Geomechanics Symposium*, Seattle, WA, USA, June.

Russell, A.R. and Wood, D.M. (2009), "Point load tests and strength measurements for brittle spheres", *Int. J. Rock Mech. Min. Sci. Geomech. Abstr.*, **46**(2), 272-280. https://doi.org/10.1016/j.ijrmms.2008.04.004.

Şahin, M., Ulusay, R. and Karakul, H. (2020), "Point load strength index of half-cut core specimens and correlation with uniaxial compressive strength", *Rock Mech. Rock Eng.*, **53**, 3745-3760. https://doi.org/10.1007/s00603-020-02137-9.

Sarici, D.E. and Ozdemir, E. (2018), "Determining point load strength loss from porosity, Schmidt hardness, and weight of some sedimentary rocks under freeze-thaw conditions", *Environ. Earth Sci.*, **77**, 1-9. https://doi.org/10.1007/s12665-018-7241-9.

Serati, M., Masoumi, H., Williams, D.J., Alehossein, H. and Roshan, H. (2018), "Some new aspects on the diametral point load testing", *The 52nd U.S. Rock Mechanics/Geomechanics Symposium*, Seattle, WA, USA, June.

Shi, Q. and Mishra, B. (2021), "Discrete element modeling of delamination in laboratory scale laminated rock", *Min. Metall. Explor.*, **38**(1), 433-446. https://doi.org/10.1007/s42461-020-00302-w.

Shi, Q., Mishra, B. and Zhao, Y. (2022), "DEM analysis of the effect of lamination properties on the stability of an underground coal mine entry with laminated shale roof", *Min. Metall. Explor.*, **39**(2), 495-506. https://doi.org/10.1007/s42461-022-00541-z.

Sternberg, E. and Rosenthal, F. (1952), "The elastic sphere under concentrated loads", *J. Appl. Mech.*, **19**(4), 413-421. https://doi.org/10.1115/1.4010536.

Timoshenko, S. (1951), *Theory of Elasticity*, McGraw-Hill Book Co., Inc., New York City, NY, UAS.

Wang, Y., Tang, J., Dai, Z. and Yi, T. (2018), "Experimental study on mechanical properties and failure modes of low-strength rock samples containing different fissures under uniaxial compression", *Eng. Fract. Mech.*, **197**, 1-20. https://doi.org/10.1016/j.engfracmech.2018.04.044.

Wei, X.X., Chau, K.T. and Wong, R.H.C. (2019), "Theoretical and experimental validation of point load strength test for irregular lumps", *J. Eng. Mech.*, **145**(9), 04019065. https://doi.org/10.1061/(ASCE)EM.1943-7889.0001638.

Wen, L., Luo, Z.Q., Yang, S.J., Qin, Y.G., Ma, S.W. and Jiang, H. (2019), "A new method for evaluating the rock mass damage index based on the field point load strength", *Royal Soc. Open Sci.*, **6**(3), 181591. https://doi.org/10.1098/rsos.181591.

Wong, R.H., Chau, K.T., Yin, J.H., Lai, D.T. and Zhao, G.S. (2017), "Uniaxial compressive strength and point load index of volcanic irregular lumps", *Int. J. Rock Mech. Min. Sci.*, **93**, 307-315. https://doi.org/10.1016/j.ijrmms.2017.02.010.

Xie, H., Wang, J.A. and Kwaśniewski, M.A. (1999), "Multifractal characterization of rock fracture surfaces", *Int. J. Rock Mech. Min. Sci.*, **36**(1), 19-27. https://doi.org/10.1016/S0148-9062(98)00172-7.

Xue, Y., Gao, D. and Mishra, B. (2018), "Stochastic simulation of rock size effect with correlation length", *The 52nd U.S. Rock Mechanics/Geomechanics Symposium*, Seattle, WA, USA, June.

Yin, J.H., Wong, R.H., Chau, K.T., Lai, D.T. and Zhao, G.S. (2017), "Point load strength index of granitic irregular lumps: Size correction and correlation with uniaxial compressive strength", *Tunn. Undergr. Space Technol.*, **70**, 388-399. https://doi.org/10.1016/j.tust.2017.09.011.

Yoon, J. (2007), "Application of experimental design and optimization to PFC model calibration in uniaxial compression simulation", *Int. J. Rock Mech. Min. Sci.*, **44**(6), 871-889. https://doi.org/10.1016/j.ijrmms.2007.01.004.

Zhang, X.P., Wu, S., Afolagboye, L.O., Wang, S. and Han, G. (2016), "Using the point load test to analyze the strength anisotropy of quartz mica schist along an exploration adit", *Rock Mech. Rock Eng.*, **49**, 1967-1975. https://doi.org/10.1007/s00603-015-0792-0.

Zhang, Y., Shao, Z., Wei, W. and Qiao, R. (2019), "PFC simulation of crack evolution and energy conversion during basalt failure process", *J. Geophys. Eng.*, **16**(3), 639-651. https://doi.org/10.1093/jge/gxz036.

HK